THE JOURNAL OF PHYSICAL CHEMISTRY B

pubs.acs.org/JPCB Article

# Confinement in Nanodiscs Anisotropically Modifies Lipid Bilayer Elastic Properties

*Published as part of The Journal of Physical Chemistry virtual special issue "Computational and Experimental Advances in Biomembranes".*

Itay Schachter, Christoph Allolio, George Khelashvili,* and Daniel Harries*

Cite This: *J. Phys. Chem. B* 2020, 124, 7166–7175 Read Online

ACCESS | Metrics & More | Article Recommendations | Supporting Information

**ABSTRACT:** Lipid nanodiscs are small synthetic lipid bilayer structures that are stabilized in solution by special circumscribing (or scaffolding) proteins or polymers. Because they create native-like environments for transmembrane proteins, lipid nanodiscs have become a powerful tool for structural determination of this class of systems when combined with cryo-electron microscopy or nuclear magnetic resonance. The elastic properties of lipid bilayers determine how the lipid environment responds to membrane protein perturbations, and how the lipid in turn modifies the conformational state of the embedded protein. However, despite the abundant use of nanodiscs in determining membrane protein structure, the elastic material properties of even pure lipid nanodiscs (i.e., without embedded proteins) have not yet been quantitatively investigated. A major hurdle is due to the inherently nonlocal treatment of the elastic properties of lipid systems implemented by most existing methods, both experimental and computational. In addition, these methods are best suited for very large "infinite" size lipidic assemblies, or ones that contain periodicity, in the case of simulations. We have previously described a computational analysis of molecular dynamics simulations designed to overcome these limitations, so it allows quantification of the bending rigidity ($K_C$) and tilt modulus ($\kappa_t$) on a local scale even for finite, nonperiodic systems, such as lipid nanodiscs. Here we use this computational approach to extract values of $K_C$ and $\kappa_t$ for a set of lipid nanodisc systems that vary in size and lipid composition. We find that the material properties of lipid nanodiscs are different from those of infinite bilayers of corresponding lipid composition, highlighting the effect of nanodisc confinement. Nanodiscs tend to show higher stiffness than their corresponding macroscopic bilayers, and moreover, their material properties vary spatially within them. For small-size MSP1 nanodiscs, the stiffness decreases radially, from a value that is larger in their center than the moduli of the corresponding bilayers by a factor of ∼2−3. The larger nanodiscs (MSP1E3D1 and MSP2N2) show milder spatial changes of moduli that are composition dependent and can be maximal in the center or at some distance from it. These trends in moduli correlate with spatially varying structural properties, including the area per lipid and the nanodisc thickness. Finally, as has previously been reported, nanodiscs tend to show deformations from perfectly flat circular geometries to varying degrees, depending on size and lipid composition. The modulations of lipid elastic properties that we find should be carefully considered when making structural and functional inferences concerning embedded proteins.

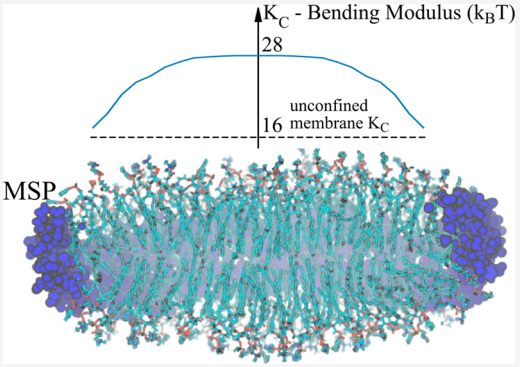


## INTRODUCTION

Lipid nanodiscs are small-size discoidal synthetic lipid bilayer structures girdled by amphiphilic scaffolding structures. The first nanodiscs were created using membrane scaffolding proteins (MSPs). These MSPs were originally designed from the ApoA1 protein component of high-density lipoprotein particles.[1,2] Because of their amphipathic character, MSPs shield the hydrophobic core of the nanodisc membrane from unfavorable exposure to the aqueous solution, thus stabilizing the nanodiscs in solution.[3] Since their introduction, a variety of other synthetic proteins and polymers of similar amphipathic nature have been developed.[4,5] This has allowed the careful optimization of MSPs for designing stable nanodiscs of well-defined size and lipid composition, in which membrane proteins could be embedded.

Because the lipid nanodisc closely resembles the environment of membrane proteins under physiological conditions,

Received: April 16, 2020
Revised: July 3, 2020
Published: July 22, 2020




https://dx.doi.org/10.1021/acs.jpcb.0c03374
*J. Phys. Chem. B* 2020, 124, 7166–7175

Table 1. Details of the Molecular Systems Simulated[a]

| environment | | lipid composition | $T$ (°C) | number of lipids | number of atoms | simulation time ($\mu$s) |
|---|---|---|---|---|---|---|
| nanodisc | MSP1E3 | POPC | 25 | 280 | 658000 | 1 |
| nanodisc | MSP1 | POPC | 25 | 176 | 350000 | 1 |
| nanodisc | MSP2N2 | POPC | 25 | 690 | 1305000 | 0.14 |
| membrane | | POPC | 25 | 256 | 57372 | 0.35 |
| nanodisc | MSP1E3 | DEPC | 25 | 286 | 560000 | 1 |
| nanodisc | MSP1 | DEPC | 25 | 180 | 351000 | 1 |
| membrane | | DEPC | 25 | 256 | 56348 | 0.5 |
| nanodisc | MSP1E3 | DLPC | 30 | 298 | 559000 | 1 |
| nanodisc | MSP1 | DLPC | 30 | 186 | 350000 | 1 |
| membrane | | DLPC | 30 | 256 | 58398 | 0.3 |
| nanodisc | MSP1E3 | DOPC | 25 | 274 | 659000 | 1 |
| nanodisc | MSP1 | DOPC | 25 | 172 | 508000 | 1 |
| membrane | | DOPC | 25 | 256 | 50216 | 0.3 |
| nanodisc | MSP1E3 | DPPC | 50 | 302 | 660000 | 1 |
| nanodisc | MSP1 | DPPC | 50 | 190 | 509000 | 1 |
| membrane | | DPPC | 50 | 190 | 64526 | 0.3 |

[a]Information is provided for each system on the lipid environment (flat periodic membrane or specific type of lipid nanodisc), lipid composition, temperature at which the simulations were run, total number of lipids, overall number of atoms, and total simulation time.

nanodiscs have found use in a number of applications, ranging from studies of biochemical and biophysical properties of membrane proteins to biotechnological and medicinal or pharmacological applications (see, for example, ref 3 and citations therein). Especially remarkable has been their role in the so-called "structural revolution".[6] Thus, when combined with cryo-electron microscopy (cryoEM) or solution nuclear magnetic resonance (NMR) spectroscopy,[7,8] lipid nanodiscs have proven to be a powerful platform for the structural determination of transmembrane proteins, with widely varying sizes and folds.[9] This technology has furthermore afforded key insights into the mechanistic role of the lipid environment in modulating the functional and structural properties of membrane proteins.[10]

Given the broad utility of lipid nanodiscs, it is not surprising that their properties have been studied extensively. Molecular dynamics (MD) simulations,[11−18] performed at either atomic or coarse-grained resolution, have been particularly useful to this end, as they have enabled important inferences regarding the structural properties of lipid nanodiscs and on how interactions between the nanodisc membrane and the surrounding MSPs stabilize these structures. For example,[12,15] studies revealed that the structural properties of pure nanodiscs (i.e., without embedded proteins) are not as uniform as they are in large "infinite"-sized lipid bilayers (represented in simulations by periodically repeating membrane patches). Instead, the nanodisc properties vary spatially, such that lipids closer to the rim of the nanodisc (i.e., closer to the MSPs) are relatively disordered (and thus present higher area per lipid (APL) and smaller bilayer thickness, $d_B$), whereas those closer to the nanodisc center are more ordered (lower APL, larger $d_B$). In fact, when investigating lipid nanodiscs composed of dipalmitoylphosphatidylcholine (DPPC) at low temperatures with atomistic MD simulations, Lopez et al.[15] observed the formation of a gel-like domain in the central region of the nanodisc, whereas around the nanodisc rim the bilayer remained in the fluid, disordered state. Consistent with these trends, the same studies also found that the configurational entropies of DPPC lipids varied locally inside the nanodisc, such that the lipids in the nanodisc center were characterized by lower entropy compared to the ones closer to the nanodisc edge.

Although detailed knowledge regarding the structural properties of lipid nanodiscs is beginning to emerge, little is known about the material properties of these systems. In particular, the curvature elastic properties of their circumscribed lipid membranes, which after all are intended to mimic free bilayers, are not resolved. This information is important because elastic properties of lipid membranes have been shown to regulate the structure−function relationships for a number of membrane proteins.[19−22] One example of such regulation has been recently demonstrated for lipid scramblase proteins in the TMEM16 family,[10] for which membrane deformations have been implicated in the functional dynamics of the protein. Indeed, the direct relation that was found between the lipid environment and the functional efficiency of the TMEM16 scramblase was attributed to the strongly slanted shape of the membrane around the protein.[10,23−25] Other examples include various transporter and channel proteins for which the membrane regulation mechanism has been related to contributions from bilayer deformation energy, curvature frustration, and lipid packing stress, among other factors (see refs 26 and 27 and citations therein). Thus, a quantitative description of the elastic properties of nanodisc membranes is potentially crucial for understanding how proteins embedded in nanodiscs are structurally and functionally influenced by the surrounding lipid environment.

The elastic properties of membranes are typically evaluated in terms of the bending rigidity ($K_C$) and lipid tilt modulus ($\kappa_t$) as defined in the Helfrich−Kozlov−Hamm free energy functional.[28−34] However, evaluating these elastic properties for nanodiscs represents a major challenge because most existing methods, both experimental and computational, that quantify these parameters, are nonlocal in nature and rely on sampling of long-range dynamic fluctuations of the lipid membrane used in conjunction with a Fourier space spectral analysis of these fluctuations.[35−40] Thus, most methods are best suited for large, effectively "infinite"-size lipidic assemblies (or in simulations, ones with periodicity) rather than for limited, finite-sized lipid bilayers, such as encountered in nanodisc membranes. We have previously introduced a


https://dx.doi.org/10.1021/acs.jpcb.0c03374
J. Phys. Chem. B 2020, 124, 7166−7175

computational analysis of MD simulations designed to overcome these limitations.[41−45] Local methods enable quantification of $K_C$ and $\kappa_t$ from local sampling of lipid splay and tilt degrees of freedom. Because it relies on the analysis of local fluctuations, this approach allows calculation of elastic moduli even for finite, nonperiodic bilayer systems.

Here we used this approach to extract $K_C$ and $\kappa_t$ elastic moduli from MD simulations performed on a set of lipid nanodisc systems varying in size and lipid composition. We find that the material properties of lipid nanodiscs are different from those of infinite bilayers of corresponding lipid composition. Moreover, the properties vary spatially within the nanodiscs, so most of the nanodiscs are softer around the edges and stiffer in the middle. Our results indicate strong correlation between the locally extracted bending rigidity and lipid area per headgroup (or bilayer thickness) that for many lipids obeys a common scaling law.[46] These modulations of lipid properties suggest that embedded proteins may also experience environments that are somewhat different in nanodiscs compared with the corresponding extended lipid bilayers. This nanodisc confinement effect should be carefully considered when making structural and functional inferences concerning embedded proteins in macroscopic lipid bilayers based on their corresponding behavior in nanodiscs.

## METHODS

**Molecular Constructs for MD Simulations.** All-atom MD simulations were carried out on two types of lipidic assemblies: (i) lipid nanodiscs of various sizes and lipid compositions and (ii) "infinite"-sized, periodic lipid bilayers with lipid compositions matching those of the nanodiscs. As detailed in Table 1, five single-component lipid systems were studied: 12:0 DLPC (1,2-dilauroyl-*sn*-glycero-3-phosphocholine), 16:0 DPPC (1,2-dipalmitoyl-*sn*-glycero-3-phosphocholine), 18:1 DOPC (1,2-dioleoyl-*sn*-glycero-3-phosphocholine), 16:0−18:1 POPC (1-palmitoyl-2-oleoyl-glycero-3-phosphocholine), and 22:1 DEPC (1,2-dierucoyl-*sn*-glycero-3-phosphocholine). For all lipids but POPC, we considered nanodiscs of two different sizes: MSP1 (diameter of ∼98 Å) and MSP1E3D1 (diameter of ∼121 Å). For POPC, we considered in addition a larger MSP2N2 nanodisc (diameter of ∼184 Å). All the nanodisc systems were constructed using the CHARMM-GUI web interface.[12,47] Figure 1A (upper panel) shows snapshots of the initial configuration of POPC nanodiscs surrounded by the three different scaffold proteins. Once assembled, the structures were placed in a cubic solution box which also contained 0.15 M KCl salt. The size of the box was chosen so that no atom of the disc was closer than 25 Å from the edge of the box. The periodic bilayers were also assembled using CHARMM-GUI. For these systems, a 30:1 ratio of water-per-lipid was used (closely corresponding to full hydration of multilamellar vesicles)[48] and 0.15 M KCl was included. The final atom-count and overall number of lipids for each nanodisc and bilayer system is shown in Table 1.

**MD Simulations Protocols and Force Fields.** All MD runs used the CHARMM36 force-field parameters for proteins,[49] lipids,[47,50] and ions.[51] The nanodisc systems were first equilibrated with NAMD version 2.12[52] using the multistep equilibration protocol available from CHARMM-GUI. This stage was followed by short (∼20 ns) unbiased MD simulations (again using NAMD). After this phase, all systems except the large POPC−MSP2N2 nanodisc were subjected to 1 $\mu$s MD simulations on the Anton2 supercomputer.[53] Due to its large size (∼1.3 million atoms, Table 1), the POPC−MSP2N2 nanodisc system could not be accommodated on the Anton2 machine and was therefore simulated with NAMD for an additional ∼140 ns.

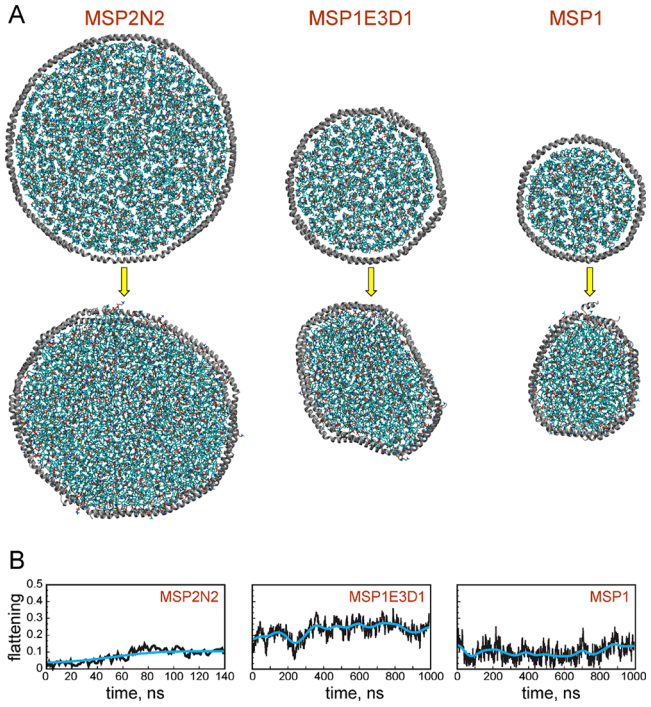


**Figure 1.** (A) Top view of the MSP2N2 (left), MSP1E3D1 (middle), and MSP1 (right) nanodiscs composed of POPC lipids, showing the discs with near-circular initial structure (top row) and time evolved structure taken from the last frame of the respective MD simulations (bottom row). The images are drawn to scale. (B) Flattening factor as a function of time corresponding to the MD simulations of the nanodiscs shown in panel A. Data is shown in black, and blue lines are Gaussian smoothing with standard deviation of 30 ns.

All the nanodisc simulations employed an isotropic pressure coupling scheme. The NAMD runs implemented a standard set of input parameters prescribed by CHARMM-GUI which includes: *vdwForceSwitching* turned on, a cutoff of 12 Å, *switchdist* 10 Å, *pairlistdist* 16 Å, PME for electrostatics,[54] Nosé-Hoover Langevin piston pressure control[55] (*langevinPistonTarget* 1.01325 bar, *langevinPistonPeriod* 50 fs, *langevinPistonDecay* 25 fs), Langevin dynamics for constant temperature control (*langevinDamping* 1 $ps^{-1}$), and an integration time step of 2 fs. The Anton2 simulations used a standard set of run parameters which included the MTK multigrator,[56] and an integration time step of 2.4 fs. Table 1 lists the temperatures at which each of the lipid system was simulated.

The corresponding bilayer systems were first equilibrated with GROMACS version 2018.3[57] using the multistep equilibration protocol prescribed by CHARMM-GUI. Then, the systems were subjected to 0.3−0.5 $\mu$s MD simulations using GROMACS. All the bilayer simulations employed a semi-isotropic pressure coupling scheme. The GROMACS runs implemented a standard set of the input parameters also prescribed by CHARMM-GUI which includes: vdw force switching turned on, cutoff 12 Å, switch distance 10 Å, PME for electrostatics, Parrinello−Rahman pressure coupling[58] (semi-isotropic pressure coupling, $\tau_p$ 5 ps, compressibility 4.5 × $10^{-5}$ $bar^{-1}$, and a pressure of 1 bar), Nosé-Hoover thermostat for constant temperature control[59] (separated for


https://dx.doi.org/10.1021/acs.jpcb.0c03374
J. Phys. Chem. B 2020, 124, 7166−7175

membrane and solution), and an integration time step of 2 fs. Table 1 lists the simulations duration and temperature.

For all systems, the analysis was performed only on the last 80% of the trajectory to ensure structural relaxation of the lipidic assemblies.

**Preparation of the Trajectories for Analysis.** In order to align the nanodiscs to a plane throughout each trajectory, the complete trajectories of the nanodisc simulations were manipulated via GROMACS and the VMD[60] RMSD (root-mean square deviation) tool to wrap the system around the nanodisc and to fit the scaffolding protein by RMSD to its initial position. For most of the trajectories all frames were fitted successfully. The few faulty ones were identified by their distinctly higher RMSD from the initial position due to improper wrapping, which could not be further mitigated. Such frames, identified with the aid of MDTraj[61] and MDAnalysis[62] packages, were discarded from subsequent analysis.

**Analysis Tools.** Properties of interest (see below) were mapped spatially on the *xy*-plane by dividing the nanodisc bilayer plane into 0.8 × 0.8 $nm^2$ sized bins, or radially (from the center-of-mass of all lipids in the nanodisc) with annuli width of 0.3 nm in order to extract the data along the radial distance from the disc center.

The APL was calculated using the Voronoi tessellation method.[63,64] To this end, we first defined the lipid positions using the center of mass (COM) of their glycerol carbonyls. This choice was found to best reproduce the APL obtained by direct calculation of the APL of continuous lipid membrane patches, simply defined by the ratio of total membrane area to number of lipids in a leaflet; see Table S1 for comparison. With this definition, a local instantaneous plane was fitted around each lipid, using neighboring lipids on the same leaflet that were within a radius of 2 nm. All the leaflet's lipid positions were projected onto this plane. Voronoi tessellation was performed on the projected plane to estimate the area of the "central" lipid for which the plane was locally fit. To mitigate edge effects, the intersection area of the Voronoi cell with the convex hull of the lipids position was used, and lipids that were positioned on the convex hull were not sampled.

The nanodisc midsurface was determined by fitting a fifth-order polynomial for the $z$ component in the Monge patch representation of the two leaflets and averaging their height. The local Gaussian and mean curvatures of these surfaces were extracted, omitting values that were a distance smaller than 0.8 nm from the in-plane convex hull.

Membrane thickness, $d_B$, was calculated as the twice the average distance of the phosphate group from the midsurface. Bending ($K_C$) and tilt ($\kappa_t$) moduli were locally calculated using the ReSiS method previously described.[44] The tilt and splay of each lipid were obtained via the Lipidator Toolkit[44] (the Toolkit is available at https://github.com/allolio/lipidator-toolkit). The extraction of the moduli also followed the implementation of ReSiS described in ref 44.

Nanodisc bilayer thickness and the lipid tilt angle with respect to the scaffolding protein (Figure S1) were calculated as a function of distance from the nanodiscs rim. Distances smaller than 0.3 nm from the protein were omitted in this calculation.

The temporal evolution of nanodisc shape was quantified by first fitting an ellipse,[65] to the convex hull of the nanodisc lipids projected onto the *xy*-plane in each trajectory frame and then calculating the flattening factor $f = (a - b)/a$, where $a$ and $b$ are the semimajor and semiminor axes of the fitted ellipse. Gaussian smoothing with standard deviation of 30 ns was used to detect longer time scale trends in flattening evolution.

Lipid diffusion was calculated by mean square displacement (MSD) time evolution. For the nanodiscs, lipids were grouped into three layers, defined by lipid initial distance from the center of mass of the disc ($d_i$) relative to the disc radius $r$ (taken from ref 12) and termed center ($d_i < 0.4r$), intermediate ($d_i \in [0.4r, 0.75r]$), and rim ($d_i > 0.75r$).

## RESULTS AND DISCUSSION

**Lipid Nanodiscs Evolve with Time into Oval-Shaped Structures.** Starting with an initial configuration that is almost perfectly round, Figure 1A upper panel, the prepared nanodiscs evolve with time into structures that are on average somewhat oval (Figure 1A, lower panel). These structures continue to fluctuate with time along the simulation trajectories. By contrast, for all nanodiscs we studied, the protein structure remained mostly intact during the simulations (see Figure S2). The changes in the nanodisc structure can be appreciated from the time evolution of the discs flattening factor, $f$, quantifying the nanodisc departure from perfectly circular geometry; see the "Methods" section. Specifically, the range of flattening is $[0, 1)$, with $f = 0$ corresponding to a perfectly circular shape, and $f \to 1$ describing a totally "flattened" ellipse (i.e., a closed curve on a line). For the three different-sized POPC systems, the flattening factor analysis, presented in Figure 1B, reveals that the medium-sized MSP1E3D1 nanodisc is characterized by somewhat larger $f$ values than either the largest MSP2N2 or the smallest MSP1 discs (note the length of the MSP2N2 trajectory is very different from the other two simulations; see Table 1). Thus, the MSP1 and MSP2N2 nanodiscs equilibrate toward shapes with flattening values in the range of $f \in [0.05, 0.15]$. The flattening factor of the MSP1E3D1 disc fluctuates at higher values, $f \in [0.2, 0.3]$. Similar departure from circular symmetry is observed also for the other lipids (Figure S3). On average, MSP1E3D1 discs show somewhat higher flattening values than the smaller MSP1 discs. Especially dramatic are deformations in the MSP1E3D1 nanodisc composed of short-tail DLPC lipids (Figure S3C), as its flattening reaches values of ∼0.35. Interestingly, the flattening of the MSP1E3D1 nanodisc composed of long-tailed DEPC lipids becomes slightly smaller with time, evolving from $f \in [0.10, 0.15]$ to $f \in [0.04, 0.07]$, suggesting that the shape of this nanodisc became almost circular.

The deviations of lipid nanodiscs from a nearly circular to oval-shaped configurations observed in our trajectories has been reported previously in MD simulations.[12] This evolution likely depends on several parameters, including the number of lipids incorporated in each nanodisc (see Table 1). We have used the judicious protocol prescribed in CHARMM-GUI for nanodisc construction (see the "Methods" section), according to which the number of lipids in a given nanodisc is determined by a combination of two factors: the nanodisc radius and the lipid headgroup area.[12] We anticipate that other choices, or indeed a polydisperse population of lipids in nanodiscs, would change many of the nanodisc properties, including the extent of deviations from circular geometries.

**Midplane of the Nanodisc Membrane Is Nonplanar.** Concomitant with their ovality, as quantified by the variation in flattening factor, we typically also find a midplane deformation of the discs. This mode of deformation can be appreciated by following the mean and Gaussian curvatures of the fitted lipid midsurface within the nanodisc (see the


https://dx.doi.org/10.1021/acs.jpcb.0c03374
J. Phys. Chem. B 2020, 124, 7166−7175

"Methods" section). For most nanodiscs we find evidence for the formation of an off-center saddle point, seen as a region of negative Gaussian curvature (Figures S4–S8). In general, when comparing MSP1 and MSP1E3D1 separately, discs with higher flattening tend to demonstrate higher out-of-plane deformations seen as larger deviations from zero curvature of the midsurface. In certain nanodiscs, such as DLPC-MSP1, highly asymmetrical curvature profiles develop during the simulations. Notably, these curvature profiles do not follow the local monolayer interface curvature, as can be derived from the membrane thickness profiles. These deformations, too, are expected to depend on lipid type, nanodisc size, lipid area density (i.e., number of lipids per nanodisc), and scaffolding protein identity.

**Structural Properties of Lipid Nanodiscs Vary Spatially.** We now turn to follow the structure and material properties of the lipid bilayer along the radial direction from the center of the lipid nanodisc. Figure 2 shows several

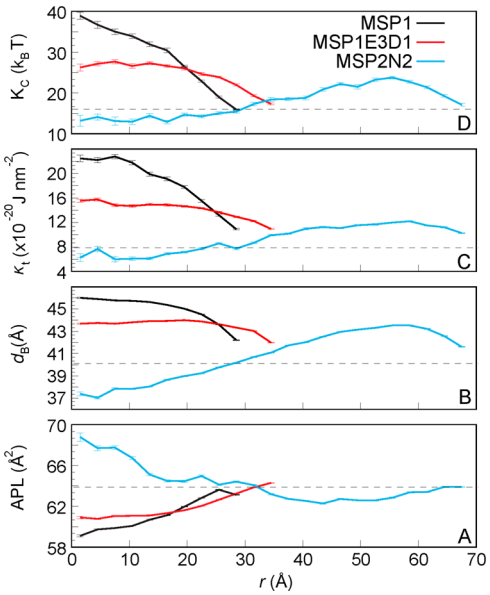


**Figure 2.** Structural and material properties of MSP1 (black line), MSP1E3D1 (red line), and MSP2N2 (blue line) nanodiscs composed of POPC lipids. Shown in ascending order (panels A–D, respectively) are monolayer area-per-lipid (APL), phosphate-to-phosphate distance ($d_B$), bilayer tilt modulus ($\kappa_t$), and bending modulus ($K_C$), as a function of radial distance from the center of the respective nanodisc. Dashed lines in each panel represent average values of the respective quantities calculated from the analysis of MD simulations of the periodic (infinite-size) POPC membranes.

structural and material properties for POPC nanodiscs of three different sizes derived from the analysis of the MD simulations. Corresponding data for 4 additional PC lipids (DLPC, DEPC, DOPC, and DPPC) is shown in Figures S9–S12. Data is plotted as a function of the radial distance, $r$, in the $xy$-plane originating from the nanodisc center: $r = 0$ corresponds to the instantaneous geometric center of the nanodisc bilayer plane, and the highest $r$ values correspond to the rim regions of each nanodisc (i.e., where the scaffolding protein start to intersect with the lipid patch, as determined by the radial distribution of protein atoms). Panels A,B of Figure 2 reveal that within each nanodisc the APL and $d_B$ vary spatially and are anticorrelated. Thus, for the two smaller nanodiscs, MSP1 and MSP1E3D1 (albeit to a lesser extent), the APL is higher around the rim of the nanodiscs and lower in the center. Correspondingly, $d_B$ is lower at the nanodisc edges and higher in the nanodisc center. This correlation between thickness and APL is expected given the incompressible (near-constant molar volume) nature of the lipid bilayer. The link between the APL and thickness is also seen in the larger MSP2N2 system, however the spatial trends are reversed, the APL being largest (thickness–smallest) at the center and smallest (thickness–largest) near the rim.

Given the observed change from convex to concave geometry at the center with increasing nanodisc size (see thickness radial profiles in Figures S9–S12), the above results suggest that nanodisc confinement drives thickening and APL reduction, that in turn increase deviations from the flat configuration as confinement is increased (by reduction of the nanodiscs radius). In other lipids, the radial variations of thickness seem to follow the general trend seen for POPC (although for DEPC-MSP1E3D1 nanodisc, the center is slightly more compressed than the corresponding MSP1 nanodisc, Figures S9–S12). These observed deviations from lipid bilayers in the flat geometry are, again, expected to be sensitively dependent on the lipid density in the nanodiscs.

Overall, the APL is lower in the nanodisc than the corresponding continuous bilayer, reflecting the more stretched and laterally compressed lipids. Exceptions are the DEPC nanodiscs that have higher APL in comparison to the bulk values, which may be related to the longer chained and unsaturated fatty acids as compared with the shorter DPPC, POPC, and DOPC lipids. In agreement with this conjecture, DLPC, which has the shortest hydrocarbon chain of the lipids we have simulated, also has lower APL around the rim. Interestingly, in the POPC nanodiscs, the APL around the rim approaches the value of the corresponding periodic flat membranes, $APL_0$ (see dashed lines in Figure 2). Correspondingly, the thickness approaches the unconfined membrane value $d_{B0}$. Notably, at the center of the nanodiscs, the APL and thickness deviate from $APL_0$, $d_{B0}$. This is also seen in DPPC and DOPC nanodiscs (Figures S11 and S12).

Due to the average deviations from circular geometry (Figure 1), the variation of the nanodisc properties is no longer solely in the radial direction. This variation can be seen in the form of "heat maps" of the structural properties of the nanodiscs in Figure 3 for POPC and S13–S16 for the rest. These figures also include a map of protein atom counts throughout the simulation to highlight the limits of lipid density and its overlap with protein densities, thus compromising lipid statistics. These figures show that, although nanodiscs are not perfectly circular, the spatial variations seen in the radial plots follow the same trends, so that a larger $d_B$ corresponds to a smaller APL and vice versa.

Lipid diffusion was also computed via the mean square displacement (MSD) of lipids in the POPC bilayer and in nanodiscs (Figure S17), as described in the "Methods" section. As seen in previous studies (e.g., see ref 12), the diffusion in the nanodisc is slower than in the bilayer. Diffusion is faster for larger discs, and largest for the periodic membrane. Surprisingly, diffusion is slower the farther the lipids are from the center of the disc, although concomitantly APL generally goes up.

**Lipid Tilt and Thickness at the Disc Boundary Determine Nanodisc Shapes.** It is well-appreciated[20,27,66–73] that the boundary conditions imposed in terms of tilting of lipids and the lipid height (or thickness) at the lipid–protein interface largely determine the shape


https://dx.doi.org/10.1021/acs.jpcb.0c03374
J. Phys. Chem. B 2020, 124, 7166–7175

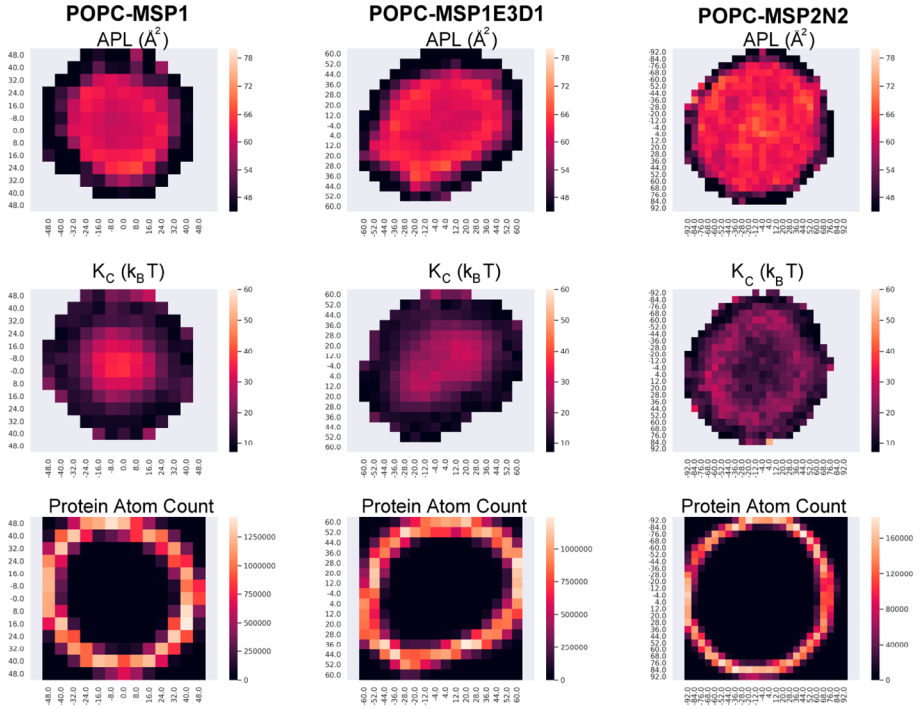


**Figure 3.** Heat maps in 2D shown for the area-per-lipid (top row), bending modulus $K_C$ (middle row), and proteins atom count (bottom row) in the simulations of MSP1 (left column), MSP1E3D1 (middle column), and MSP2N2 (right column) nanodiscs composed of POPC lipids.

profile of lipid membranes near and away from the protein inclusions. The effect of the nanodisc boundary can be readily recognized from simulation snapshots (Figure S18), where we find considerable lipid deformations close to the rim. Thus, to further probe the effect of confinement, we examined bilayer thickness near the rim (Figure 4A) as compared to the bilayer thickness in the corresponding periodic membrane, and the tilt angle $\theta$ of lipids near the rim (Figure 4B). See Figure S1 on how the tilt angle is calculated; radial profiles from the rim to the disc center for both quantities are shown in Figure S19. For most nanodiscs, lipid thickness at the rim is similar to that of the corresponding periodic membrane "bulk" values, but values depend on chain length and lipid saturation. Specifically, the longer (DEPC) or shorter (DLPC) tailed lipids seem to adjust so as to accommodate the resulting hydrophobic mismatch. Lipids at the nanodisc rim are on average tilted with respect to the scaffolding protein (Figure 4B), with a range $\theta \in [0.25, 0.37]$ (positive values indicating that the lipids are tilted toward the protein). The combined effect of boundary values of tilt and thickness is to force a curved height profile for lipid nanodiscs. Overall, as distance from the protein scaffold grows, thickness increases up to some maximal value and then slightly decreases (Figure S19), leading to a general increase in lipid thickness due to nanodisc confinement. Exceptions are DLPC−MSP1E3D1 and POPC−MSP2N2, where we find a decrease in thickness after the maxima. Due to this decrease, the membrane thickness comes close to that of the continuous bilayer or even slightly decreases below it close to the nanodisc center for the largest nanodisc. Because, by symmetry, in the nanodisc center the tilt angles reach the bulk value of 0 (Figure S19), we find that shorter lipids (DLPC and DPPC) that have smaller tilt angles at the rim also relax faster to zero. Underscoring the strong confinement of the nanodiscs, tilt angles relax to the bulk values within a typical distance of ∼1.3−2.0 nm, comparable to the radii of the MSP1 and

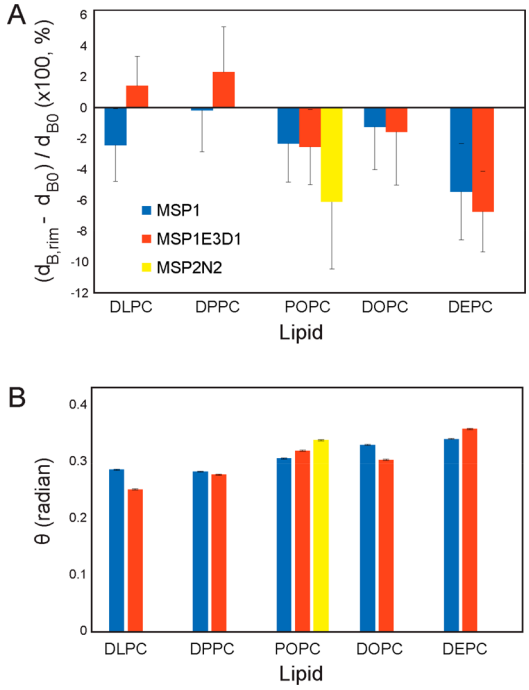


**Figure 4.** Thickness and tilt of lipids at the scaffolding protein boundary. (A) Bar plot of the change in rim thickness relative to corresponding periodic bilayer of the various lipid systems. (B) Bar plot of the near-rim tilt angle for the various lipids and discs. Rim lipids defined here as those residing 0.3−0.6 nm from the rim.

MSP1E3D1 nanodiscs themselves. This results in smaller discs generally not relaxing to the free membrane values even in the center of the nanodisc that is furthest from the rim. The combined lipid tilt and thickness can cause lipid stretching or contraction; indeed, we find that for all lipids the near-rim lipid


https://dx.doi.org/10.1021/acs.jpcb.0c03374
J. Phys. Chem. B 2020, 124, 7166−7175

length is larger than the near-rim thickness by at least 3−6%, depending on the lipid, with shorter lipids stretching more.

**Local Changes in Elastic Moduli of Lipid Nanodiscs Correlate with Structural Variations.** Remarkably, we found that the observed spatial variation in the structural properties of the nanodiscs, both APL and $d_B$, is mirrored by changes in the local elastic properties. Indeed, as shown in Figure 2, for MSP1 and MSP1E3D1 POPC nanodiscs, the $K_C$ values vary locally from lowest (softer) at the nanodisc rim to highest (most rigid) at its center, with these trends being larger for MSP1. The $K_C$ values in the center are ∼2−3 fold higher than those for the corresponding bilayers, reflecting a significant stiffening of lipids due to nanodisc confinement. Moreover, for most nanodiscs (Figures S9−S12), $K_C$ is higher throughout the entire nanodisc, thus suggesting that under confinement nanodisc lipid patches are stiffer as a whole than unconfined membranes.

For the MSP2N2 system, the trend in $K_C$ is reversed. It is highest at the rim and lowest at the center, so $K_C$ values in the central region of this disc are similar to that found in the regular periodic POPC bilayers (dashed lines in Figure 2). The observed positive correlation between $K_C$ and thickness (and negative correlation between $K_C$ and APL) is not surprising, since it reflects the generally accepted view that thicker bilayers are more rigid.[45]

For all lipids (Figures 2 and S9−S12), the tilt moduli $\kappa_t$ show the same general trends as the bending moduli. The deviations of the various lipids from their unconfined membrane properties and the general stiffening of all but the largest nanodisc of MSP2N2 are due to the nanodiscs' confinement effect. This effect is driven by the finite nanometric system size together with the boundary effects imposed by the girdling proteins, as well as by the constant and small number of lipids. Under these constraints, the system minimizes its free energy, reaching specific equilibrium shape and properties. If the system size is large enough to allow relaxation from the boundary conditions at the rim, then properties in the center of the nanodisc will approach their known membrane unconstrained bulk values, as observed here for the MSP2N2 nanodisc (Figure 2). However, for strong confinement as seen in the smaller nanodiscs, spatial relaxation to bulk values is prohibited, and deviations from the large membranes is expected.

**Variation of Local $K_C$ with APL in Nanodiscs Follows Known General Scaling Law for Lipid Membranes.** The data described in Figures 2 and S8−S11 suggests a strong correlation between $K_C$ and APL (or thickness). This finding is interesting in light of the known general relationship between these quantities for lipid membranes. Thus, using mean field theory[46] it has previously been shown that the variation of $K_C$ with APL approximately follows a power law $K_C(\mathrm{APL}) \sim (\mathrm{APL})^{-7}$. In our previous simulations of periodic membranes of different lipid compositions, we found the same relationship between $K_C$ and APL.[45] To test whether the same scaling holds in lipid nanodiscs, we studied the relationship between spatial variations in $K_C$ and APL in the nanodisc systems. To this end, using the heat map data for each system, we paired local values for $K_C$ and APL corresponding to the same bin (excluding near-rim bins). Then, we plotted $\log(K_C/K_C^{max})$ as a function of $\log(\mathrm{APL}/\mathrm{APL}^{min})$ for each lipid separately (i.e., merging data for all the discs for a specific lipid). Here, $\mathrm{APL}^{min}$ and $K_C^{max}$ are normalization factors that correspond, respectively, to the smallest APL and largest $K_C$ of the used values. To the resulted scatter data, shown in Figure 5, we fitted a power law of the form $\log(K_C/K_C^{max}) = -m \times \log(\mathrm{APL}/\mathrm{APL}^{min}) + C$ (see dashed lines in Figure 5). We found that the value of the fitted exponent, $m$, ranged between 6.3 and 7.0 for all lipids with saturated tails (DLPC, DPPC, and POPC; see Figure 5 captions), but for the unsaturated lipids (DOPC, DEPC) the values were lower (3.4 for DOPC and 5.6 for DEPC). These results suggest that the same general scaling law, derived for global properties of homogeneous lipid membranes whose properties on average are spatially homogeneous, is also closely applicable to the nanodisc systems with saturated lipids, where $K_C$ and APL vary spatially.

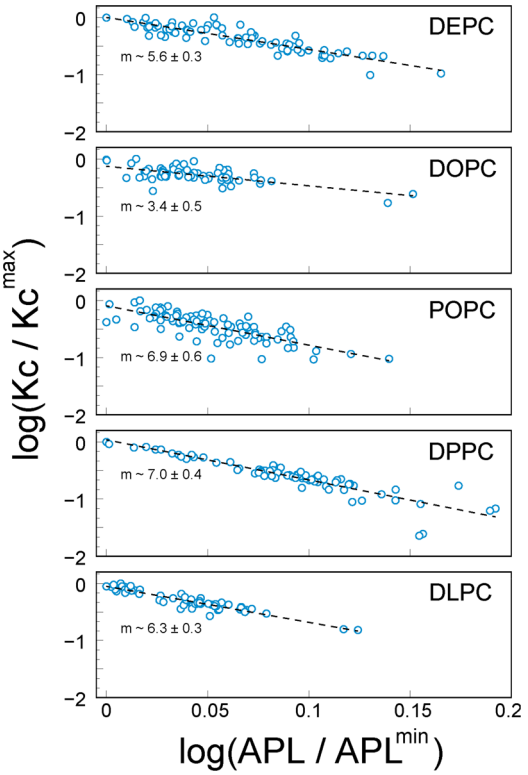


**Figure 5.** Scaling relation for bending modulus of different lipids. Figures show $\log(K_C/K_C^{max})$ as a function of $\log(APL/APL^{min})$ for different lipid nanodisc systems. For each lipid composition, all the nanodisc systems were analyzed. Panels show, as circles, paired local values for the two logarithms corresponding to the same bin from the heat maps (see text for more details). Dashed lines show a power law fits of the form $\log(K_C/K_C^{max}) = -m \times \log(APL/APL^{min}) + C$ to the resulted scattered data. Values of the linear slope fit coefficient ($m$) for each case are also indicated.

## CONCLUSIONS

Using MD simulations, we have presented a systematic study of structural and material properties of various lipid nanodiscs differing in size and lipid composition. The computational analysis tool we have recently developed was used here to extract the spatially resolved elastic moduli from MD trajectories of finite-size nanodisc structures. The analysis revealed that for a given lipid type all the measured properties (i.e., area per lipid, bilayer thickness, bending rigidity, and tilt modulus) varied within each nanodisc and between nanodiscs of different sizes. Moreover, the nanodiscs are significantly stiffer than their corresponding unconstrained (periodic)


https://dx.doi.org/10.1021/acs.jpcb.0c03374
J. Phys. Chem. B 2020, 124, 7166−7175

membranes. The results indicate strong correlation between the locally extracted bending rigidity and area per lipid (or bilayer thickness) that obey a common scaling law. Our findings may have implications as to how proteins embedded in nanodiscs can be structurally and functionally influenced by properties of the surrounding lipid environment.

## ■ ASSOCIATED CONTENT

### Supporting Information

The Supporting Information is available free of charge at https://pubs.acs.org/doi/10.1021/acs.jpcb.0c03374.

Structural details for additional lipids (DEPC, DOPC, DPPC, and DLPC) in various nanodiscs. Table with structural properties of continuous bilayers. (PDF)

## ■ AUTHOR INFORMATION


### Corresponding Authors

**Daniel Harries** − *Institute of Chemistry, the Fritz Haber Research Center, and the Harvey M. Kruger center for Nanoscience & Nanotechnology, The Hebrew University, Jerusalem 9190401, Israel;* orcid.org/0000-0002-3057-9485; Email: daniel.harries@mail.huji.ac.il

**George Khelashvili** − *Department of Physiology and Biophysics and Institute for Computational Biomedicine, Weill Cornell Medical College of Cornell University, New York, New York 10065, United States;* orcid.org/0000-0001-7235-8579; Email: gek2009@med.cornell.edu

### Authors

**Itay Schachter** − *Institute of Chemistry, the Fritz Haber Research Center, and the Harvey M. Kruger center for Nanoscience & Nanotechnology, The Hebrew University, Jerusalem 9190401, Israel;* orcid.org/0000-0003-4517-4090

**Christoph Allolio** − *Institute of Mathematics, Faculty of Mathematics and Physics, Charles University, Prague 18674, Czech Republic;* orcid.org/0000-0002-7525-9266

Complete contact information is available at: https://pubs.acs.org/10.1021/acs.jpcb.0c03374


### Notes

The authors declare no competing financial interest.

## ■ ACKNOWLEDGMENTS

I.S. thanks the Harvey M. Kruger center for Nanoscience & Nanotechnology for their fellowship. C.A. acknowledges support from Charles University project grant PRIMUS/20/SCI/015. G.K. gratefully acknowledges support from the 1923 Fund. D.H. thanks the financial support from the Israel Science Foundation (ISF grant No. 1246/17). The computational work was performed using the following resources: the computational resources of the David A. Cofrin Center for Biomedical Information in the HRH Prince Alwaleed Bin Talal Bin Abdulaziz Alsaud Institute for Computational Biomedicine at Weill Cornell Medical College; Anton 2 supercomputer provided by the Pittsburgh Supercomputing Center (PSC) through Grant R01GM116961 from the National Institutes of Health; and the computational facility at the Fritz Haber Center at the Hebrew University. The Anton 2 machine at PSC was generously made available by D. E. Shaw Research. The Fritz Haber Research Center is supported by the Minerva Foundation, Munich, Germany.

## ■ REFERENCES


(1) Davidson, W. S.; Hilliard, G. M. The spatial organization of apolipoprotein A-I on the edge of discoidal high density lipoprotein particles: a mass specrometry study. *J. Biol. Chem.* **2003**, *278* (29), 27199−207.

(2) Li, Y.; Kijac, A. Z.; Sligar, S. G.; Rienstra, C. M. Structural analysis of nanoscale self-assembled discoidal lipid bilayers by solid-state NMR spectroscopy. *Biophys. J.* **2006**, *91* (10), 3819−28.

(3) Denisov, I. G.; Sligar, S. G. Nanodiscs in Membrane Biochemistry and Biophysics. *Chem. Rev.* **2017**, *117* (6), 4669−4713.

(4) Ritchie, T. K.; Grinkova, Y. V.; Bayburt, T. H.; Denisov, I. G.; Zolnerciks, J. K.; Atkins, W. M.; Sligar, S. G. Chapter 11 - Reconstitution of membrane proteins in phospholipid bilayer nanodiscs. *Methods Enzymol.* **2009**, *464*, 211−31.

(5) Dorr, J. M.; Scheidelaar, S.; Koorengevel, M. C.; Dominguez, J. J.; Schafer, M.; van Walree, C. A.; Killian, J. A. The styrene-maleic acid copolymer: a versatile tool in membrane research. *Eur. Biophys. J.* **2016**, *45* (1), 3−21.

(6) Callaway, E. Revolutionary cryo-EM is taking over structural biology. *Nature* **2020**, *578* (7794), 201.

(7) Hagn, F.; Etzkorn, M.; Raschle, T.; Wagner, G. Optimized phospholipid bilayer nanodiscs facilitate high-resolution structure determination of membrane proteins. *J. Am. Chem. Soc.* **2013**, *135* (5), 1919−25.

(8) Hagn, F.; Nasr, M. L.; Wagner, G. Assembly of phospholipid nanodiscs of controlled size for structural studies of membrane proteins by NMR. *Nat. Protoc.* **2018**, *13* (1), 79−98.

(9) Grinkova, Y. V.; Denisov, I. G.; Sligar, S. G. Engineering extended membrane scaffold proteins for self-assembly of soluble nanoscale lipid bilayers. *Protein Eng., Des. Sel.* **2010**, *23* (11), 843−8.

(10) Khelashvili, G.; Cheng, X.; Falzone, M. E.; Doktorova, M.; Accardi, A.; Weinstein, H. Membrane lipids are both the substrates and a mechanistically responsive environment of TMEM16 scramblase proteins. *J. Comput. Chem.* **2020**, *41* (6), 538−551.

(11) Pourmousa, M.; Pastor, R. W. Molecular dynamics simulations of lipid nanodiscs. *Biochim. Biophys. Acta, Biomembr.* **2018**, *1860*, 2094.

(12) Qi, Y.; Lee, J.; Klauda, J. B.; Im, W. CHARMM-GUI Nanodisc Builder for modeling and simulation of various nanodisc systems. *J. Comput. Chem.* **2019**, *40* (7), 893−899.

(13) Pourmousa, M.; Song, H. D.; He, Y.; Heinecke, J. W.; Segrest, J. P.; Pastor, R. W. Tertiary structure of apolipoprotein A-I in nascent high-density lipoproteins. *Proc. Natl. Acad. Sci. U. S. A.* **2018**, *115* (20), 5163−5168.

(14) Shih, A. Y.; Denisov, I. G.; Phillips, J. C.; Sligar, S. G.; Schulten, K. Molecular dynamics simulations of discoidal bilayers assembled from truncated human lipoproteins. *Biophys. J.* **2005**, *88* (1), 548−56.

(15) Lopez, C. A.; Swift, M. F.; Xu, X. P.; Hanein, D.; Volkmann, N.; Gnanakaran, S. Biophysical Characterization of a Nanodisc with and without BAX: An Integrative Study Using Molecular Dynamics Simulations and Cryo-EM. *Structure* **2019**, *27* (6), 988−999.

(16) Siuda, I.; Tieleman, D. P. Molecular models of nanodiscs. *J. Chem. Theory Comput.* **2015**, *11* (10), 4923−32.

(17) Debnath, A.; Schafer, L. V. Structure and Dynamics of Phospholipid Nanodiscs from All-Atom and Coarse-Grained Simulations. *J. Phys. Chem. B* **2015**, *119* (23), 6991−7002.

(18) Augustyn, B.; Stepien, P.; Poojari, C.; Mobarak, E.; Polit, A.; Wisniewska-Becker, A.; Rog, T. Cholesteryl Hemisuccinate Is Not a Good Replacement for Cholesterol in Lipid Nanodiscs. *J. Phys. Chem. B* **2019**, *123* (46), 9839−9845.

(19) Andersen, O. S.; Koeppe, R. E., 2nd Bilayer thickness and membrane protein function: an energetic perspective. *Annu. Rev. Biophys. Biomol. Struct.* **2007**, *36*, 107−30.

(20) Mondal, S.; Khelashvili, G.; Weinstein, H. Not Just an Oil Slick: How the Energetics of Protein-Membrane Interactions Impacts the Function and Organization of Transmembrane Proteins. *Biophys. J.* **2014**, *106* (11), 2305−2316.

(21) Phillips, R.; Ursell, T.; Wiggins, P.; Sens, P. Emerging roles for lipids in shaping membrane-protein function. *Nature* **2009**, *459* (7245), 379−85.
(22) Simunovic, M.; Voth, G. A.; Callan-Jones, A.; Bassereau, P. When Physics Takes Over: BAR Proteins and Membrane Curvature. *Trends Cell Biol.* **2015**, *25* (12), 780−792.
(23) Falzone, M.; Rheinberger, J.; Lee, B. C.; Peyear, T.; Sasset, L.; Raczkowski, A.; Eng, E.; Di Lorenzo, A.; Andersen, O. S.; Nimigean, C. M.; Accardi, A. Structural basis of Ca2+-dependent activation and lipid transport by a TMEM16 scramblase. *eLife* **2019**, *8* (pii), e43229.
(24) Alvadia, C.; Lim, N. K.; Clerico Mosina, V.; Oostergetel, G. T.; Dutzler, R.; Paulino, C. Cryo-EM structures and functional characterization of the murine lipid scramblase TMEM16F. *eLife* **2019**, *8*, e44365.
(25) Kalienkova, V.; Clerico Mosina, V.; Bryner, L.; Oostergetel, G. T.; Dutzler, R.; Paulino, C. Stepwise activation mechanism of the scramblase nhTMEM16 revealed by cryo-EM. *eLife* **2019**, *8*, e44364.
(26) Lundbaek, J. A.; Collingwood, S. A.; Ingolfsson, H. I.; Kapoor, R.; Andersen, O. S. Lipid bilayer regulation of membrane protein function: gramicidin channels as molecular force probes. *J. R. Soc., Interface* **2010**, *7* (44), 373−95.
(27) Bezrukov, S. Functional consequences of lipid packing stress. *Curr. Opin. Colloid Interface Sci.* **2000**, *5* (3−4), 237−243.
(28) Helfrich, W. Elastic properties of lipid bilayers: theory and possible experiments. *Z. Naturforsch., C: J. Biosci.* **1973**, *28* (11), 693−703.
(29) Canham, P. B. The minimum energy of bending as a possible explanation of the biconcave shape of the human red blood cell. *J. Theor. Biol.* **1970**, *26* (1), 61−81.
(30) Evans, E. A. Bending resistance and chemically induced moments in membrane bilayers. *Biophys. J.* **1974**, *14* (12), 923−31.
(31) May, S.; Kozlovsky, Y.; Ben-Shaul, A.; Kozlov, M. M. Tilt modulus of a lipid monolayer. *Eur. Phys. J. E: Soft Matter Biol. Phys.* **2004**, *14* (3), 299−308.
(32) Fosnaric, M.; Iglic, A.; May, S. Influence of rigid inclusions on the bending elasticity of a lipid membrane. *Phys. Rev. E Stat Nonlin Soft Matter Phys.* **2006**, *74*, 051503.
(33) Kozlovsky, Y.; Kozlov, M. M. Stalk model of membrane fusion: solution of energy crisis. *Biophys. J.* **2002**, *82* (2), 882−95.
(34) Hamm, M.; Kozlov, M. M. Elastic energy of tilt and bending of fluid membranes. *Eur. Phys. J. E: Soft Matter Biol. Phys.* **2000**, *3* (4), 323−335.
(35) Watson, M. C.; Brandt, E. G.; Welch, P. M.; Brown, F. L. Determining biomembrane bending rigidities from simulations of modest size. *Phys. Rev. Lett.* **2012**, *109* (2), 028102.
(36) Watson, M. C.; Penev, E. S.; Welch, P. M.; Brown, F. L. Thermal fluctuations in shape, thickness, and molecular orientation in lipid bilayers. *J. Chem. Phys.* **2011**, *135* (24), 244701.
(37) Hofsass, C.; Lindahl, E.; Edholm, O. Molecular dynamics simulations of phospholipid bilayers with cholesterol. *Biophys. J.* **2003**, *84* (4), 2192−206.
(38) Lindahl, E.; Edholm, O. Mesoscopic undulations and thickness fluctuations in lipid bilayers from molecular dynamics simulations. *Biophys. J.* **2000**, *79* (1), 426−33.
(39) Brandt, E. G.; Braun, A. R.; Sachs, J. N.; Nagle, J. F.; Edholm, O. Interpretation of Fluctuation Spectra in Lipid Bilayer Simulations. *Biophys. J.* **2011**, *100*, 2104.
(40) Nagle, J. F. Experimentally determined tilt and bending moduli of single-component lipid bilayers. *Chem. Phys. Lipids* **2017**, *205*, 18−24.
(41) Johner, N.; Harries, D.; Khelashvili, G. Implementation of a methodology for determining elastic properties of lipid assemblies from molecular dynamics simulations. *BMC Bioinf.* **2016**, *17*, 161.
(42) Johner, N.; Harries, D.; Khelashvili, G. Curvature and Lipid Packing Modulate the Elastic Properties of Lipid Assemblies: Comparing HII and Lamellar Phases. *J. Phys. Chem. Lett.* **2014**, *5* (23), 4201−6.
(43) Khelashvili, G.; Kollmitzer, B.; Heftberger, P.; Pabst, G.; Harries, D. Calculating the Bending Modulus for Multicomponent Lipid Membranes in Different Thermodynamic Phases. *J. Chem. Theory Comput.* **2013**, *9* (9), 3866−3871.
(44) Allolio, C.; Haluts, A.; Harries, D. A local instantaneous surface method for extracting membrane elastic moduli from simulation: Comparison with other strategies. *Chem. Phys.* **2018**, *514*, 31−43.
(45) Doktorova, M.; Harries, D.; Khelashvili, G. Determination of bending rigidity and tilt modulus of lipid membranes from real-space fluctuation analysis of molecular dynamics simulations. *Phys. Chem. Chem. Phys.* **2017**, *19* (25), 16806−16818.
(46) Szleifer, I.; Kramer, D.; Benshaul, A.; Gelbart, W. M.; Safran, S. A. Molecular Theory of Curvature Elasticity in Surfactant Films. *J. Chem. Phys.* **1990**, *92* (11), 6800−6817.
(47) Wu, E. L.; Cheng, X.; Jo, S.; Rui, H.; Song, K. C.; Davila-Contreras, E. M.; Qi, Y.; Lee, J.; Monje-Galvan, V.; Venable, R. M.; Klauda, J. B.; Im, W. CHARMM-GUI Membrane Builder toward realistic biological membrane simulations. *J. Comput. Chem.* **2014**, *35* (27), 1997−2004.
(48) Tristram-Nagle, S. A. Preparation of oriented, fully hydrated lipid samples for structure determination using X-ray scattering. *Methods Mol. Biol.* **2007**, *400*, 63−75.
(49) Best, R. B.; Zhu, X.; Shim, J.; Lopes, P. E.; Mittal, J.; Feig, M.; Mackerell, A. D., Jr. Optimization of the additive CHARMM all-atom protein force field targeting improved sampling of the backbone phi, psi and side-chain chi(1) and chi(2) dihedral angles. *J. Chem. Theory Comput.* **2012**, *8* (9), 3257−3273.
(50) Klauda, J. B.; Venable, R. M.; Freites, J. A.; O'Connor, J. W.; Tobias, D. J.; Mondragon-Ramirez, C.; Vorobyov, I.; MacKerell, A. D.; Pastor, R. W. Update of the CHARMM All-Atom Additive Force Field for Lipids: Validation on Six Lipid Types. *J. Phys. Chem. B* **2010**, *114* (23), 7830−7843.
(51) Venable, R. M.; Luo, Y.; Gawrisch, K.; Roux, B.; Pastor, R. W. Simulations of anionic lipid membranes: development of interaction-specific ion parameters and validation using NMR data. *J. Phys. Chem. B* **2013**, *117* (35), 10183−92.
(52) Phillips, J. C.; Braun, R.; Wang, W.; Gumbart, J.; Tajkhorshid, E.; Villa, E.; Chipot, C.; Skeel, R. D.; Kale, L.; Schulten, K. Scalable molecular dynamics with NAMD. *J. Comput. Chem.* **2005**, *26* (16), 1781−1802.
(53) Shaw, D. E.; Grossman, J. P.; Bank, J. A.; Batson, B.; Butts, J. A.; Chao, J. C.; Deneroff, M. M.; al, e. Anton 2: Raising the Bar for Performance and Programmability in a Special-Purpose Molecular Dynamics Supercomputer. *IEEE* **2014**, 41−53.
(54) Essmann, U.; Perera, L.; Berkowitz, M. L.; Darden, T.; Lee, H.; Pedersen, L. G. A Smooth Particle Mesh Ewald Method. *J. Chem. Phys.* **1995**, *103* (19), 8577−8593.
(55) Feller, S. E.; Zhang, Y. H.; Pastor, R. W.; Brooks, B. R. Constant-Pressure Molecular-Dynamics Simulation - the Langevin Piston Method. *J. Chem. Phys.* **1995**, *103* (11), 4613−4621.
(56) Martyna, G. J.; Tobias, D. J.; Klein, M. L. Constant-Pressure Molecular-Dynamics Algorithms. *J. Chem. Phys.* **1994**, *101* (5), 4177−4189.
(57) Van der Spoel, D.; Lindahl, E.; Hess, B.; Groenhof, G.; Mark, A. E.; Berendsen, H. J. C. GROMACS: Fast, flexible, and free. *J. Comput. Chem.* **2005**, *26* (16), 1701−1718.
(58) Parrinello, M.; Rahman, A. Polymorphic Transitions in Single-Crystals - a New Molecular-Dynamics Method. *J. Appl. Phys.* **1981**, *52* (12), 7182−7190.
(59) Evans, D. J.; Holian, B. L. The Nose-Hoover Thermostat. *J. Chem. Phys.* **1985**, *83* (8), 4069−4074.
(60) Humphrey, W.; Dalke, A.; Schulten, K. VMD: visual molecular dynamics. *J. Mol. Graphics* **1996**, *14* (1), 33−8.
(61) McGibbon, R. T.; Beauchamp, K. A.; Harrigan, M. P.; Klein, C.; Swails, J. M.; Hernandez, C. X.; Schwantes, C. R.; Wang, L. P.; Lane, T. J.; Pande, V. S. MDTraj: A Modern Open Library for the Analysis of Molecular Dynamics Trajectories. *Biophys. J.* **2015**, *109* (8), 1528−32.
(62) Gowers, R.; Linke, M.; Barnoud, J.; Reddy, T.; Melo, M.; Seyler, S.; Domanski, J.; Dotson, D.; Buchoux, S.; Kenney, I.; Beckstein, O. MDAnalysis: A Python Package for the Rapid Analysis


https://dx.doi.org/10.1021/acs.jpcb.0c03374
J. Phys. Chem. B 2020, 124, 7166−7175

of Molecular Dynamics Simulations. *Python in Science Conference* **2016**, 98.
(63) Aurenhammer, F. Voronoi diagrams - a survey of a fundamental geometric data structure. *ACM Computing Surveys* **1991**, *23* (3), 345−405.
(64) Virtanen, P.; Gommers, R.; Oliphant, T. E.; Haberland, M.; Reddy, T.; Cournapeau, D.; Burovski, E.; Peterson, P.; Weckesser, W.; Bright, J.; et al. SciPy 1.0: fundamental algorithms for scientific computing in Python. *Nat. Methods* **2020**, *17* (3), 261−272.
(65) Hammel, B.; Sullivan-Molina, N. bdhammel/least-squares-ellipse-fitting: Initial release. https://zenodo.org/record/2578663#.XozKsnJ7lQK.
(66) May, S.; Ben-Shaul, A. Molecular theory of lipid-protein interaction and the $L_{\alpha}$-$H_{II}$ transition. *Biophys. J.* **1999**, *76* (2), 751−767.
(67) Mondal, S.; Khelashvili, G.; Shi, L.; Weinstein, H. The cost of living in the membrane: A case study of hydrophobic mismatch for the multi-segment protein LeuT. *Chem. Phys. Lipids* **2013**, *169*, 27−38.
(68) Mondal, S.; Khelashvili, G.; Shan, J.; Andersen, O. S.; Weinstein, H. Quantitative modeling of membrane deformations by multi-helical membrane proteins: Application to G-protein Coupled Receptors. *Biophys. J.* **2011**, *101*, 2092−2101.
(69) Lundbaek, J. A.; Andersen, O. S.; Werge, T.; Nielsen, C. Cholesterol-induced protein sorting: An analysis of energetic feasibility. *Biophys. J.* **2003**, *84* (3), 2080−2089.
(70) Nielsen, C.; Goulian, M.; Andersen, O. S. Energetics of inclusion-induced bilayer deformations. *Biophys. J.* **1998**, *74* (4), 1966−83.
(71) Marsh, D. Protein modulation of lipids, and vice-versa, in membranes. *Biochim. Biophys. Acta, Biomembr.* **2008**, *1778* (7−8), 1545−75.
(72) Marsh, D. Energetics of hydrophobic matching in lipid-protein interactions. *Biophys. J.* **2008**, *94* (10), 3996−4013.
(73) de Planque, M. R.; Killian, J. A. Protein-lipid interactions studied with designed transmembrane peptides: role of hydrophobic matching and interfacial anchoring. *Mol. Membr. Biol.* **2003**, *20* (4), 271−284.


https://dx.doi.org/10.1021/acs.jpcb.0c03374
*J. Phys. Chem. B* 2020, 124, 7166−7175